Visualization of Highly Ordered Striated Domains Induced by Transmembrane Peptides in Supported Phosphatidylcholine Bilayers†

Hilde A. Rinia,*,‡,§ Richard A. Kik,‡ Rudy A. Demel,‡ Margot M. E. Snel,§ J. Antoinette Killian,‡ Jan P. J. M. van der Eerden,§ and Ben de Kruijff‡

Department of Biochemistry of Membranes, Institute of Biomembranes, CBLE, and Department of Interfaces, Debye Institute, Utrecht University, Padualaan 8, 3584 CH, Utrecht, The Netherlands.

Received January 4, 2000; Revised Manuscript Received March 2, 2000

ABSTRACT: We used atomic force microscopy (AFM) to study the lateral organization of transmembrane $TmAW_2(LA)_nW_2Etn$ peptides (WALP peptides) incorporated in phospholipid bilayers. These well-studied model peptides consist of a hydrophobic alanine−leucine stretch of variable length, flanked on each side by two tryptophans. They were incorporated in saturated phosphatidylcholine (PC) vesicles, which were deposited on a solid substrate via the vesicle fusion method, yielding hydrated gel-state supported bilayers. At low concentrations (1 mol %) WALP peptides induced primarily line-type depressions in the bilayer. In addition, striated lateral domains were observed, which increased in amount and size (from 25 nm up to 10 μm) upon increasing peptide concentration. At high peptide concentration (10 mol %), the bilayer consisted mainly of striated domains. The striated domains consist of line-type depressions and elevations with a repeat distance of 8 nm, which form an extremely ordered, predominantly hexagonal pattern. Overall, this pattern was independent of the length of the peptides (19−27 amino acids) and the length of the lipid acyl chains (16−18 carbon atoms). The striated domains could be pushed down reversibly by the AFM tip and are thermodynamically stable. This is the first direct visualization of α-helical transmembrane peptide−lipid domains in a bilayer. We propose that these striated domains consist of arrays of WALP peptides and fluidlike PC molecules, which appear as low lines. The presence of the peptides perturbs the bilayer organization, resulting in a decrease in the tilt of the lipids between the peptide arrays. These lipids therefore appear as high lines.

Lateral segregation of proteins and lipids in biological membranes is commonly assumed to give rise to biologically differentiated regions (*1*−*4*). Segregation processes would lead to the formation of domains and the length scales of these domains may be as small as 10−100 nm, which is difficult to detect with most experimental techniques (*5*).

Fluorescence microscopy studies have already demonstrated the existence of lipid domains in cell membranes (*6*). However, the resolution of this technique is relatively low and the presence of probes is required. The resolution of electron microscopy is much higher, and lateral phase separation yielding microdomains has been observed in biomembranes and model membranes with freeze−fracturing techniques (*7*, *8*). A drawback of this technique is that it demands quenching of the sample, which could lead to structural reorganization. Computer simulations can visualize the distribution of individual molecules in model bilayers (*5*, *9*). Monte Carlo simulations have suggested that proteins can induce lipid sorting in binary lipid bilayers (*10*, *11*) and that lipids in turn, can cause clustering of proteins (*12*, *13*).

Atomic force microscopy (AFM)[1] (*14*) offers the possibility to directly image phospholipid bilayers on a solid support, under aqueous conditions (*15*, *16*), while the resolution (0.5−1 nm) (*17*) is sufficient to directly visualize domains of mesoscopic size. Indeed, domains have been observed by AFM. In dipalmitoylphosphatidylcholine (DPPC) monolayers, intermixed liquid expanded and liquid crystalline lipid domains as small as 500 nm have been imaged (*18*). Also interdigitated domains, induced by alcohol (*19*) or heat (*20*), have been visualized in DPPC bilayers. From AFM images of binary mixtures of dipalmitoylphosphatidylethanolamine and the cholera toxine receptor ganglioside, it was concluded that such bilayers phase-separate, forming small domains (*16*). Also, protein aggregation in lipid monolayers (*21*) has been observed. Amphipathic peptides were found to induce round domains and filaments in fluid phosphatidylcholine (PC) monolayers (*22*) and interdigitated domains in DPPC bilayers (*23*). In a thorough AFM study, Mou et al. (*24*) have reported on the aggregation behavior of gramicidin A (GA), which is known to span bilayers as a β-helical dimer. They were able to visualize line-type GA aggregates in supported gel-state PC bilayers, and these aggregates clustered together

† This work was supported by the Division of Chemical Sciences with financial aid from The Netherlands Organization for Scientific Research (N.W.O.)

* Corresponding author: CBLE, Utrecht University, P.O. Box 80054, Padualaan 8, 3508 TB, Utrecht, The Netherlands. Telephone 31-30-2533211; Fax 31-30-2522478; E-mail h.rinia@chem.uu.nl.

‡ Institute of Biomembranes, CBLE.

§ Debye Institute.

[1] Abbreviations: AFM, atomic force microscopy; PC, phosphatidylcholine; DOPC, 1,2-dioleoyl-*sn*-glycero-3-phosphocholine; DPPC, 1,2-dipalmitoyl-*sn*-glycero-3-phosphocholine; DSPC, 1,2-distearoyl-*sn*-glycero-3-phosphocholine; WALP, tryptophan−alanine−leucine peptide $FmAW_2(LA)_nW_2AEtn$; TFE, trifluoroethanol; GA, gramicidin A; H_{II}, inverse hexagonal lipid phase.

10.1021/bi000010c CCC: $19.00
Published on Web 04/22/2000

Table 1: Amino Acid Sequences of the WALP Peptides and Their Estimated Total Length, When Present as an α-Helix

peptide	amino acid sequence	total length[a] (nm)
WALP16	Ac-GWW$(LA)_5$WWA-$NHCH_2CH_2OH$	2.5
WALP19	Ac-GWWL$(AL)_6$WWA-$NHCH_2CH_2OH$	3.0
WALP23	Ac-GWWL$(AL)_8$WWA-$NHCH_2CH_2OH$	3.6
WALP27	Ac-GWWL$(AL)_{10}$WWA-$NHCH_2CH_2OH$	4.2

[a] Assuming each amino acid has a length of 0.15 nm, with the C-terminal ethanolamine included as the length of one amino acid (26).

in ordered domains. These findings prove that AFM is indeed a powerful tool to study lateral segregation in bilayers. Although the hydrophobic transmembrane domains of integral membrane proteins, interacting with the hydrophobic core of the surrounding lipid membrane, usually consist of α-helices, none of the above-mentioned AFM studies concern proteins with an α-helical transmembrane domain.

To systematically study the interactions of such α-helices with the surrounding lipid membrane, synthetic transmembrane model peptides are commonly used (*25*). An example of such peptides are the WALP peptides (*26*), which consist of an alternating alanine−leucine stretch of variable length and form a hydrophobic α-helix. The peptides are flanked on both ends by two tryptophans. These residues are often found in membrane-spanning proteins at the hydrophobic−hydrophilic interface of the bilayer (*27*). WALP peptides have mainly been used to study the effect of mismatch between the hydrophobic transmembrane regions of integral membrane proteins and the hydrophobic core of the lipid bilayer. Such hydrophobic mismatch is thought to have an important effect on lateral segregation in membranes (*2*), on membrane protein activity and stability, and on protein sorting (*25*, *28*). It has been found that WALP peptides can induce the formation of the H_{II} phase in fluid PC bilayers (*26*) and alter the thickness of fluid PC bilayers (*29*).

The aim of our study is to visualize possible lateral segregation of these α-helical, transmembrane model peptides in phospholipid bilayers. WALP peptides give us the opportunity to systematically vary the length of the peptides and to investigate possible effects of mismatch on the aggregation behavior of these peptides in gel-state bilayers. We found that WALP peptides in supported PC bilayers segregate in highly ordered striated domains and that they have a distinct influence on the organization of the surrounding lipids.

MATERIALS AND METHODS

1,2-Dipalmitoyl-*sn*-glycero-3-phosphocholine (DPPC) and 1,2-distearoyl-*sn*-glycero-3-phosphocholine (DSPC) were purchased from Avanti Polar Lipids (Alabaster, AL) and used without any further purification. WALP peptides consist of a hydrophobic alanine−leucine stretch of variable length flanked by tryptophans. To avoid complications due to electrostatics, the N- and C-terminus are blocked with an acetyl group and an ethanolamine group, respectively. Table 1 shows the amino acid sequences and the lengths of the different WALP peptides we used. All WALP peptides were synthesized essentially as described (*26*) and were a kind gift of Drs. Roger E. Koepe II and Denise V. Greathouse.

2,2,2-Trifluoroethanol (TFE) was from Sigma (St. Louis, MO). For all experiments MilliQ water was used.

Vesicle Preparation. The peptides were dissolved in TFE and added to DPPC or DSPC dissolved in a mixture of chloroform and methanol (3:1 v/v). The obtained peptide/lipid mixtures contained 1, 2, 5, or 10 mol % peptide. These mixtures were dried in a rotary evaporator followed by overnight storage under high vacuum. To the dried mixed films was added 1.25 mL of a 20 mM NaCl solution, resulting in a lipid concentration of 0.62 mM. After 10 cycles of freeze−thawing, small unilamellar vesicles were made by sonicating the suspension in a bath sonicator (Branson, Danbury, CT) at maximum power for at least 30 min, at 50 °C (in the case of DPPC) or 65 °C (in the case of DSPC). Possible remaining large vesicles were spun down at 20800*g* for 1 h, at 4 °C. The resulting vesicle suspensions had a pH of 6 and were used within 10 days after preparation.

Preparation of Supported Bilayers. Vesicle suspension (75 μL) was applied onto freshly cleaved mica (∅ 10 mm), glued on a steel disk coated around the mica with hydrophobic silicone sealant (Sigma Coatings, Uithoorn, Holland). The vesicles were allowed to adsorb to the mica for at least 10 h at 4 °C, as described (*24*). After the sample was rinsed with 5−10 times 75 μL of 20 mM NaCl, the sample was heated above the main transition temperature of the lipids present (to 60 °C for DPPC and 70 °C for DSPC) for 45 min. Afterward, the sample was left to cool to room temperature at ambient conditions, which usually took less than 15 min, and rinsed again with 5−10 times 75 μL of 20 mM NaCl. In this way bilayers were obtained, usually containing defects and with some unopened vesicles on top. Occasionally, the bilayers were partly covered by a second bilayer, which, when imaged by AFM, appeared hazy and contaminated. The images presented in the results section are of the first bilayer. Care was taken that the samples remained hydrated. To investigate the thermodynamic stability of the bilayers, some samples of 2 mol % WALP23 in DPPC were, after they had been heated, either cooled very quickly by immediately applying cold solution (4 °C), or were left to cool very slowly, at a rate of 10 °C per hour. Unless stated otherwise, all samples were scanned a few hours after preparation.

AFM Measurements. The sample was mounted on an E-scanner, which was calibrated on a standard grid, of a Nanoscope III (Digital Instruments, Santa Barbara, CA). A quartz flow cell was used without the O-ring. All samples were scanned with oxide-sharpened tips with a spring constant of 0.06 N/m, as estimated by the manufacturer (Digital Instruments, Santa Barbara, CA). Scans were recorded at a minimal force where the image was stable and clear, which was usually smaller than 500 pN, and with a scan speed of 6 lines/s. To investigate the compressibility of the samples, in some cases the scanning force was increased up to 1500 pN.

The AFM software was used to measure distances within an image and to perform Fourier transformations. All images shown in this paper, except for the inset in Figure 2, are flattened raw data.

RESULTS

In all presented AFM images, differences in height are visible as differences in gray tones. In this scale, black is low, and white is high.

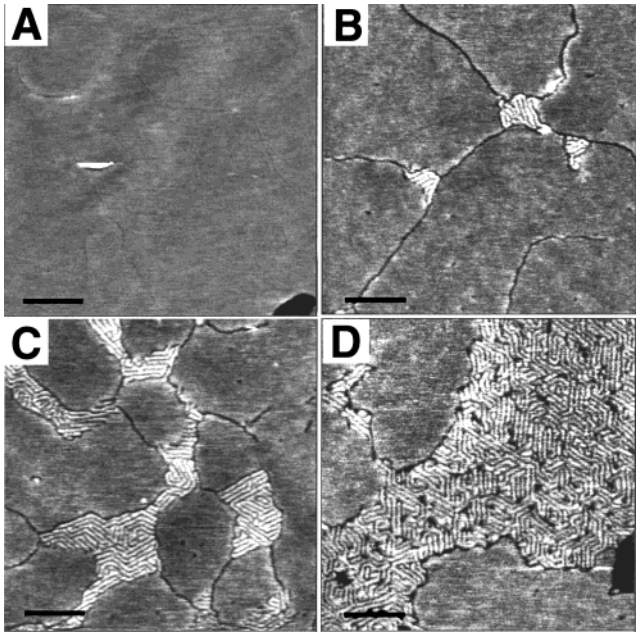

FIGURE 1: Formation of striated domains induced by WALP23 in DPPC bilayers. AFM images of (A) a pure DPPC gel-state bilayer, image size 1 × 1 μm, scale bar 200 nm; (B) a bilayer of DPPC with 1 mol % WALP23 incorporated; (C) a bilayer of DPPC with 2 mol % WALP23 incorporated; and (D) a bilayer of DPPC with 5 mol % WALP23. Image sizes of B−D are 500 × 500 nm, scale bar 100 nm.

WALP23 in DPPC. Pure DPPC (Figure 1A) bilayers have a smooth appearance with a few defects, in agreement with previous studies (*15*, *24*). Occasionally shallow cracks can be seen in the bilayer surface, with a depth of less than 0.1 nm. Figure 1B depicts a bilayer of DPPC with 1 mol % WALP23 incorporated. Distinct line-type depressions appear that are flanked by slightly higher areas, and occasionally, small pointlike depressions are present. Also small striated domains can be seen, usually where more than two line-type depressions meet. These domains consist of low (dark) and high (light) lines. Increasing the concentration of WALP23 to 2 mol % (Figure 1C) again resulted in pointlike and line-type depressions and in larger striated domains in which the lines curve at defined angles. Upon incorporation of 5 mol % WALP23 (Figure 1D), even larger striated domains are formed in which small defects are present. Bilayers of DPPC with 10 mol % WALP23 incorporated consisted almost completely of striated domains, which sometimes occupied areas as large as 100 μm^2. Figure 2 depicts an image at larger magnification of such a domain, which clearly shows that in the striated domains the lines curve in angles of 120°, showing a 3-fold symmetry. The Fourier transformation of this domain is shown in the inset. This power spectrum displays a hexagonal pattern, consistent with the angles of 120°, found in the original pattern. Fourier transformations of large striated domains formed at 2 or 5 mol % gave the same results. The average repeat distance as deduced from power spectra of the striated domains and as determined directly from the images was found to be 7.5 ± 0.4 nm (n = 27). The width and the depth of the isolated line-type depressions in WALP23 containing DPPC bilayers were about 9 and 0.3 nm respectively, and the height of the higher areas along these depressions varied between 0.1 and 0.3 nm, taking the bilayer surface as the zero level.

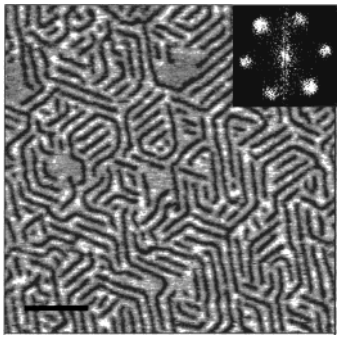

FIGURE 2: AFM image at high magnification of a striated domain, formed in a bilayer of DPPC with 10 mol % WALP23. Image size 250 × 250 nm and scale bar 50 nm. The inset shows the power spectrum made of this domain, from which it is deduced that the average angle between the lines in the domains is 60°, and their average distance is 7.5 nm.

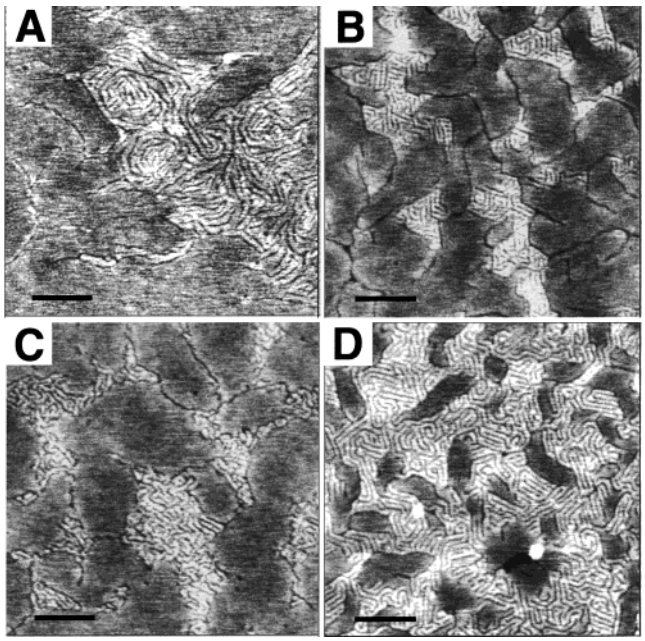

FIGURE 3: Domains of WALP peptides of varying lengths, formed in PC bilayers. (A) WALP16 (2 mol %) in DPPC, image size 1 × 1 μm, scale bar 200 nm. (B) WALP19 (2 mol %) in DPPC. (C) WALP27 (5 mol %) in DPPC. (D) WALP23 (5 mol %) in DSPC. Image sizes of B−D are 500 × 500 nm, scale bar = 100 nm.

Other WALPs and Lipids. To investigate the importance of the length of the peptide and lipid acyl chains for domain formation, bilayers of DPPC (C_{16}) with WALP16, WALP19, and WALP27 and of DSPC (C_{18}) with WALP23 were imaged. In all DPPC bilayers with WALP incorporated, pointlike and line-type depressions appeared, the latter with a width and a depth of about 9 and 0.3 nm respectively, flanked by higher areas, varying between 0.1 and 0.3 nm (taking the bilayer surface as the zero level). Also in these systems striated domains are observed.

In the case of WALP16 incorporated in DPPC bilayers, the amount of line-type depressions increased with increasing peptide concentration. Often, but not always, striated domains could be seen. Figure 3A shows an example of such a domain formed in a bilayer of DPPC with 2 mol % WALP16 (note that the scale is larger compared to the WALP19, -23, and -27 images). These domains also consist of low lines separated by higher areas, but the distance between the line-type depressions is larger [23 ± 4 nm (n = 26)] as compared

Table 2: Total Bilayer Thickness and Hydrophobic Bilayer Thickness of DPPC and DSPC in the Gel and Fluid Phase, in Excess Water.

lipid	bilayer thickness (nm)	hydrophobic bilayer thickness (nm)
DPPC (gel)	4.7[a]	3.6[b]
DPPC (fluid)	3.7[c]	2.6[c]
DSPC (gel)	4.7[a]	3.6[b]
DSPC (fluid)	4.1[c]	3.0[c]

[a] Values for the total bilayer thickness of PC in the gel phase are adopted from ref *30*. The tilt angle of the acyl chains in a DPPC gel-state bilayer is 33°, and in a DSPC gel-state bilayer, 40°. [b] Value for the hydrophobic bilayer thickness of DPPC in the gel phase is adopted from ref 28, and for DSPC (following ref 28) 1.1 nm is subtracted from the total measured length. [c] Values for the total and hydrophobic bilayer thickness of PC in the fluid phase are adopted from ref 31.

to the repeat distance of the lines in the striated domains formed in bilayers containing WALP23. Also, the period is not as well-defined as in the case of WALP23 in DPPC and the lines do not usually curve at specific angles.

When WALP19 or WALP27 was incorporated in DPPC bilayers, striated domains were present, of which the amount and size increased with increasing peptide concentration. Figure 3B shows an image of striated domains formed in a DPPC bilayer with WALP19 (2 mol %) incorporated. The period of the lines in such patterns is 8.2 ± 0.5 nm ($n = 9$), as measured directly from the images. The pattern of these striated domains has the same appearance as the pattern of the striated domains induced by WALP23, albeit that the lines look somewhat straighter and the curves sharper. When WALP27 was incorporated, striated domains were formed as depicted in Figure 3C (5 mol % WALP27 in DPPC). The period, as measured directly from the images, was 7.9 ± 0.9 nm ($n = 10$). The pattern differs merely slightly from the pattern of the striated domains in the bilayers containing WALP23, in that the lines seem less straight and curve at less defined angles. Also, for both WALP19 and WALP27, it was more difficult to obtain sharp images of the striated domains; hence we were not able to reliably determine the angle and period from Fourier transformations.

The use of DSPC, with saturated acyl chains of 18 carbon atoms long, instead of DPPC, with saturated acyl chains of 16 carbon atoms, did not distinctly influence the pattern of the striated domains either. This can be seen in Figure 3D, which shows striated domains in a bilayer of DSPC with 5 mol % WALP23 incorporated. The period of the lines in the pattern was found to be 8.1 ± 0.7 nm ($n = 7$).

The thickness of the bilayers was determined by using the largest defects already present in the bilayer (*23*). The thickness of the DPPC bilayer outside the striated domains was 5.8−5.9 nm, independent of the length of the incorporated peptide. The bilayer thickness as measured by AFM is larger than the DPPC bilayer thickness given in Table 2, because presumably there is a layer of 1−2 nm of water between the supported bilayer and the substrate (*15*).

Imaging fluid bilayers with peptides incorporated, yielded images without contrast, which is in agreement with the findings of Mou et al. (*24*). This could be attributed to the high compressibility of the fluid bilayers (*24*) or to the rapid movement of the molecules present in such systems.

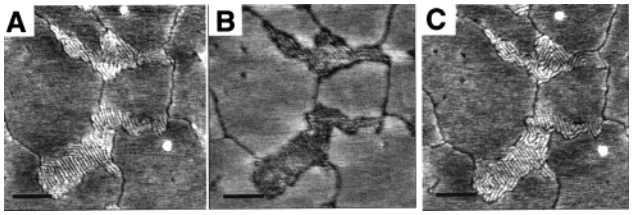

FIGURE 4: Striated domains (2 mol % WALP23 in DPPC) imaged at different forces. (A) At low force (<500 pN), the domains appear higher than the surrounding bilayer. (B) Upon increasing the force to 1500 pN, the domains are pushed down. (C) At low force (<500 pN), the domains appear high again.

Examining the Striated Domains. The height of the striated domains was dependent on the force applied by the tip. When during scanning the force was low (<500 pN), the height of the striated domains varied between 0.2 and 0.4 nm, taking the bilayer surface as the zero level. This was found for WALP19, -23 and -27 in DPPC and for WALP23 in DSPC. Upon increasing the force, the striated domains could be pushed down. Figure 4A shows an example of striated domains in a system of WALP23 in DPPC, imaged at low force (<500 pN). When the scanning force was increased to 1500 pN, the striated domains appear below the surface of the bilayer (Figure 4B). When afterward the force was decreased again, the height and the pattern of the striated domains reappeared (Figure 4C). Note that also the higher areas along the line-type depressions disappear at higher force (Figure 4B) and reappear at low force (Figure 4C).

To determine whether the striated domains are thermodynamically stable, some samples of 2 mol % WALP23 in DPPC were, after they had been heated to 60 °C, cooled quickly and some were left to cool slowly. In the systems that had been cooled quickly, domains were present (data not shown) with the same pattern as presented above (Figure 1C), although on the whole, the striated domains seemed somewhat smaller in the quenched sample. In the samples that were cooled slowly (10 °C/h), again striated domains could be seen (data not shown) with the same pattern as the systems with WALP23, cooled at ambient conditions. However, the domains seemed larger and had the appearance of the striated domains in 5 mol % WALP23 in DPPC (Figure 1D). Some samples of 2 mol % WALP23 in DPPC were imaged after they had cooled at ambient conditions and subsequently had been left at room temperature for 2 days. The pattern of the domains in these systems was again the same (data not shown) as in the bilayers imaged within a few hours after cooling.

These results indicate that the striated domains are flexible and thermodynamically stable.

DISCUSSION

Formation of Line-Type Depressions. In the systems we studied with WALP peptides at low concentrations, mainly line-type depressions were observed (Figure 1B). All WALP peptides have a smaller length than the bilayer thickness of DPPC and DSPC in the gel phase (see Table 2). Moreover, tryptophans are known to preferentially locate at the interface of the lipid headgroups and acyl chains (*32*), which would keep the peptides below the surface of the bilayer. Hence we assume that, in the line-type depressions, peptides are residing. The measured depth of the line-type depressions

in the bilayers with WALP peptides of different length does not differ much from one WALP peptide to another (all about 0.3 nm). We suspect this to be due to the fact that the lines (measured width ± 9 nm) are too narrow for the tip (radius ± 10 nm) to reach "the bottom" of the depressions, and that therefore differences in depth due to differences in peptide length could not be detected.

We suggest the following explanation for the formation of the line-type depressions: In pure DPPC bilayers, sometimes shallow line-type depressions or cracks can be seen in the surface (Figure 1A). We believe that these cracks are borders between different domains in the gel-state bilayers. In DPPC layers in the gel state, the lipid acyl chains are tilted at a 33° angle (*30*) and are short-range, hexagonally ordered. When the fluid bilayer is cooled during the preparation (from above to below the phase transition temperature), the lipids will start to solidify at different sites within the bilayer, leading to the formation of different domains. Within each domain the lipid acyl chains are tilted in the same direction, which might be different from the direction of the lipids in the neighboring domain. This would lead to disordered boundaries. We have discussed this principle for a DPPC monolayer in a previous study (*33*).

When peptides are present in a solidifying PC bilayer, they might not be incorporated in the ordered lipid domains but rather be "squeezed out" of those domains, so that they end up in the disordered boundaries (this mechanism is comparable to surface enrichments of contaminations in a crystal). This would explain the line-type depressions in the PC bilayers with 1 or 2 mol % peptide incorporated, as shown in Figures 1B,C and Figure 3A−C.

Unlike in pure DPPC bilayers (Figure 1A), sometimes isolated small pointlike depressions can be seen in the gel-state domains in the mixed bilayers (Figure 1B,C, and 3C, and 4), wherein possibly also peptides are residing. It could be that not all the peptide is excluded from the DPPC gel-state domains into the line-type depressions and that some peptide is present as small pointlike aggregates in the bilayer.

The measured width of the line-type depressions is 9 nm, but due to the tip convolution the real width is probably even larger. This is larger than the diameter of an α-helix, which is estimated to be 1 nm (*27*). Proteins and peptides are known to be able to change the state of the neighboring (annular) lipids from gel to more fluidlike (*12*, *34*). These fluidlike annular phospholipids would also appear lower than phospholipids in the gel state. Hence we expect that the line-type depressions consist of arrays of peptides (possibly more than one peptide wide), which are bordered by fluidlike, disordered PC lipids.

The line-type depressions are flanked by slightly higher areas (0.1−0.3 nm) (Figures 1B,C, 3A−C, and 4A,C). These higher areas appeared usually along every line-type defect we observed, especially at low force. Theoretical studies have predicted a possible local larger bilayer thickness around inclusions, like proteins and peptides (*35*), even in case of hydrophobic matching (*36*). We speculate that these elevations are a result of packing constraints in the bilayer, caused by the presence of the peptides (see also below).

Formation and Composition of the Striated Domains. We suggest that when there is more peptide present than can be accommodated in the boundaries, striated domains are formed, often at the intersection of three or more lines (Figures 1B,C and 3B,C). It could be that the disordered boundaries serve as channels along which the peptides are transported to the growing striated domain, during solidification of the mixed bilayer.

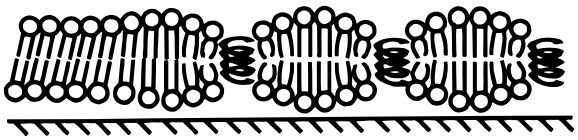

FIGURE 5: Proposed model for the molecular organization in the striated domains. The tilted packing of saturated PC in the gel phase (left) is disturbed by the presence of the peptides, depicted as coiled springs. This results in disorder and in a decrease in tilt of the lipids between the peptide arrays; hence they appear higher, and have a larger compressibility than the bulk gel-state bilayer.

The height difference between the striated domains and the bulk bilayer is too small for the Nanoscope software to quantify the percentage of area occupied by striated domains. However, from the images of the bilayers with 10 mol % WALP23, it is easy to see by eye that these bilayers consist almost completely of striated domains. In the striated domains themselves (Figure 2), half of the area is low (dark lines) and the other half is high (white lines). This means that almost 50% of the area in the bilayers with 10 mol % WALP23 consists of low lines. Assuming one PC headgroup occupies 0.5 nm^2 (*30*) and one α-helix 0.8 nm^2 [diameter is 1 nm (*27*)], in a DPPC bilayer containing 10 mol % WALP23, only 25% of the area would be occupied by protein. From this it follows that the area taken up by the low lines in the domains cannot consist completely of peptide, simply because there is not enough peptide present. This implies, analogous to the isolated line-type depressions, the presence of phospholipids in a more fluidlike phase, which would also appear below the level of the gel-state bilayer.

We propose that the organization of the lipids and the peptides in the striated domains is comparable to the organization in the line-type depressions. The domains consist of arrays of peptide, flanked by phospholipids in a fluidlike state, observed as low lines. The width of these low lines in the domains is extremely constant, suggesting that the peptide lines consist of arrays of constant peptide units: either monomers or oligomers. Since the formation of WALP oligomers is unlikely (*29*), we think that the low lines in the striated domains consist of arrays of peptide monomers.

In the striated domains the bilayer is perturbed by the presence of inclusions in the form of peptide arrays. These inclusions make it impossible for the surrounding lipids to pack in a tilted conformation, as they prefer at gel-state temperature. Since these lipids appear in our AFM images as elevated lines, we assume that they are present with a decreased or no tilt. Figure 5 depicts a possible model of the molecular organization in the striated domains (on the right) and the neighboring gel-state bilayer (on the left). In the lipid phase between the peptide arrays, the lipids are more disordered and thus have a higher compressibility compared to the lipids in the gel-state bilayer. This would explain the fact that the striated domains can be pushed down (reversibly) below the level of the bulk bilayer (Figure 4).

Pattern of the Striated Domains. We have compared the striking pattern of the domains with resembling patterns

described in the literature, to gain more insight in why the lipids and peptides would form such ordered stripes.

Binary systems undergoing spinodal decomposition (*37*), also form a pattern of alternating lines. Such systems are thermodynamically unstable. It could be that in the striated domains the lipids and peptides are on their way to phase separation. During this process the width of the lines would continuously increase. However, because the domains still exhibit the same pattern after 2 days (data not shown), and the bilayers that were cooled very slowly (10 °C/h) exhibited striated domains with the same periodicity (data not shown), we regard it unlikely that the pattern we see in the striated domains originates from a mixture of peptides and lipids undergoing spinodal decomposition.

Seul and Andelman (*38*) give an analysis of domain shapes and striped (or bubbled) patterns, referred to as modulated phases. These patterns occur in various thermodynamically stable systems and are the result of a compromise between competing interactions in these systems. From their overview (38) it follows that striated patterns induced in membranes, vesicles, and bilayers find their origin in curvature and molecular tilt, but this applies to pure phospholipid systems. The period of the described systems can be tuned by varying involved parameters, like temperature, concentration, and the length of the phospholipid tails. For example, the period of ripples in phospholipid systems in the $P_{\beta'}$ phase is determined by the acyl chain length of the lipids present. In our case, the period remains constant when the length of the lipid acyl chains or peptides is varied (except for WALP16). So, even though the morphology of the ripple phase resembles the pattern of the striated domains in the 3-fold symmetry of the ripples and lines, we exclude the possibility that the striated domains we observe are bilayer areas in the $P_{\beta'}$ phase.

Recently it was found by Vlot and van der Eerden (*39*), using Monte Carlo computer simulations, that in binary systems of enantiomers, striated phases were formed when steric hindrance was introduced, denoted as spaghetti solid or spaghetti liquid. When the optimum distance or steric hindrance between the two components increased, the system became more liquid, being expressed as lines that are more curved, while the width of the lines remained the same. Thus, geometrical factors influenced only the line stiffness. WALP19, -23, and -27 are estimated to be longer than the hydrophobic thickness of fluid DPPC (Tables 1 and 2), so when the peptide length increases from 19 to 27 amino acids, the hydrophobic mismatch between the peptides and their supposedly neighboring phospholipids would also increase. Also, going from WALP19 to WALP27, the lines in the striated domains get less straight and the angles at which the lines curve get less sharp (Figure 3B,C). Analogous to the spaghetti phases, an increase in mismatch may decrease the line stiffness, while the width of the lines remains constant. However, in our systems also specific interactions, like the preference of tryptophans to anchor at the headgroup−tail interface of the bilayer, could be involved in the striated pattern formation. Therefore the spaghetti phase should not be considered as an accurate model for our system but merely as an indication that geometrical factors could be involved in the pattern formation.

The results we obtained in this study have some striking similarities with the study of Mou et al. (*24*) on gramicidin A (GA) in saturated PC bilayers. GA is a β-helical peptide, which spans the bilayer as a dimer. Also this hydrophobic peptide induces line-type depressions in gel-state PC bilayers, and at higher concentration (2 mol %) domains are observed. Along the line-type depressions higher areas appear, and the domains are higher than the surrounding bilayer. The pattern of the domains observed in the presence of GA consists of pointlike depressions surrounded by percolating line-type depressions. As in our systems, the line-type depressions in the domains tend to curve at angles of 120°. It was suggested that this is reflecting the arrangement of the peptide in the depressions, which is thought to be as hexamers (*24*, *40*). However, there are no indications that the WALP peptides used in the current study would form hexamers, and yet, defined angles of 120° are observed. Since in these two studies different peptides (GA and WALPs) are used, we deduce that the observed hexagonality is either directed by the lipids or by general geometrical packing properties of the system.

Also notable is that the distance between the line-type depressions within the domains induced by both peptides is similar (for WALP19, 27 ± 4 nm, and for GA, 4.7 nm). It may seem counterintuitive that the length scale of the bilayer deformations is independent of the chemistry and the geometry of the inclusions. However, according to a theoretical study of Nielsen et al. (*35*), it is the rigidity of the bilayer that largely influences this length scale.

From the above, we conclude that most likely general geometrical factors of both lipids and peptides and elastic properties of the lipid bilayer are involved in the formation of the striated domain pattern.

Computer simulations of peptides or proteins in lipid bilayers usually show the formation of clusters or aggregates of the proteins (*9*, *12*). The peptides or proteins may be ordered within the aggregate, forming 2-D crystals (*13*); however, to our knowledge, line-type aggregates forming an ordered pattern within the lipid phase have never been observed, also not in simulations concerning proteins in gel-state bilayers (*12*). AFM images as presented in this study provide small-scale experimental pictures, potentially guiding theoreticians doing computational studies on peptide−lipid aggregation.

In conclusion, we have found that transmembrane α-helical peptides in gel-state DPPC bilayers form line-type aggregates and that these aggregates cluster together in striated domains, which in most cases are unexpectedly highly ordered. This ability to form highly ordered structures might have implications for the organization in biological membranes. In future work, we will investigate the role of the tryptophans in the formation of the domains by varying the flanking residues.

ACKNOWLEDGMENT

We thank Drs. Roger E. Koeppe II and Denise V. Greathouse for kindly providing the WALP peptides, G. J. K. van den Berg for skillful technical assistance, and Dr. Margot J. Vlot for helpful discussions.

REFERENCES

1. Welti, R., and Glaser, M. (1994) *Chem. Phys. Lipids 73*, 121−137.
2. Mouritsen, O. G., and Bloom, M. (1984) *Biophys. J. 46*, 141−153.
3. Vaz, W. L. C. (1994) *Biophys. Chem. 50*, 139−145.

4. Simons, K., and Ikonen, E. (1997) *Nature 387*, 569−572.
5. Mouritsen, O. G., and Biltonen, R. L. (1993) in *Protein−Lipid Interactions* (Watts, A., Ed.) p 1−39, Elsevier, Amsterdam.
6. Haverstick, D. M., and Glaser, M. (1987) *Proc. Natl. Acad. Sci. U.S.A. 84*, 4475−4479.
7. Verkleij, A. J. (1989) in *Electron Microscopy of Subcellular Dynamics*, (Plattner, H., Ed.) pp 75−94, CRC, Boca Raton, FL.
8. Luna, E. J., and McConnell, H. M. (1978) *Biochim. Biophys. Acta 509*, 462−473.
9. Gil, T., Ipsen, J. H., Mouritsen, O. G., Sabra, M. C., Sperotto, M. M., and Zuckermann, M. J. (1998) *Biochim. Biophys. Acta 1376*, 245−266.
10. Sperotto, M. M., and Mouritsen, O. G. (1993) *Eur. Biophys. J. 22*, 323−328.
11. Dumas, F., Sperotto, M. M., Lebrun, M. C., Tocanne, J.-F., and Mouritsen, O. G. (1997) *Biophys. J. 73*, 1940−53.
12. Sperotto, M. M., and Mouritsen, O. G. (1991) *Eur. Biophys. J. 19*, 157−168.
13. Sabra, M. C., Uitdehaag, J. C. M., and Watts, A. (1998) *Biophys. J. 75*, 1180−1188.
14. Binnig, G., Quate, C. F., and Gerber, Ch. (1986) *Phys. Rev. Lett. 56*, 1007−1022.
15. Tamm, L. K., and Shao, Z. (1998) in *Biomembrane Structures*, (Harris, P. I., and Chapman, D., Eds.) pp 169−185, IOS Press, Amsterdam.
16. Yang, J., Tamm, L. K., Somlyo, A. P., and Shao, Z. (1993) *J. Microsc. 171*, 183−198.
17. Engel, A., Schoenenberger, C.-A., and Müller, D. J. (1997) *Curr. Opin. Struct. Biol. 7*, 279−284.
18. Hollars, C. W., and Dunn, R. C. (1998) *Biophys. J. 75*, 342−353.
19. Mou, J., Yang, J., Huang, C., and Shao, Z. (1994) *Biochemistry 33*, 9981−9985.
20. Fang, Y., and Yang, J. (1997) *Biochim. Biophys. Acta 1324*, 309−319.
21. Amrein, M., von Nahmen, A., and Sieber, M. (1997) *Eur. Biophys. J. 26*, 349−357.
22. Van Mau, N, Vie, V., Chaloin, L., Lesniewska, E., Heitz, F., and Le Grimellec, C. (1999) *J. Membr. Biol. 167*, 241−249.
23. Janshoff, A., Bong, D. T., Steinem, C., Johnson, J. E., and Ghadiri, M. R. (1999) *Biochemistry 38*, 5328−5336.
24. Mou, J., Czajkowsky, D. M., and Shao, Z. (1996) *Biochemistry 35*, 3222−3226.
25. Killian, J. A. (1998) *Biochim. Biophys. Acta 1376*, 401−416.
26. Killian, J. A., Salemink, I., de Planque, M. R. R., Lindblom, G., Koeppe, R. E., II, and Greathouse, D. V. (1996) *Biochemistry 35*, 1037−1045.
27. Reithmeier, R. A. F. (1995) *Curr. Opin. Struct. Biol. 5*, 491−500.
28. Dumas, F., Lebrun, M. C., and Tocanne, J.-F. (1999) *FEBS Lett. 458*, 271−277.
29. De Planque, M. R. R., Greathouse, D. V., Koeppe, R. E., II, Schäfer, H., Marsh, D., and Killian, J. A. (1998) *Biochemistry 37*, 9333−9345.
30. Marsh, D. (1990) *Handbook of Lipid Bilayers*, CRC, Boca Raton, FL.
31. Lewis, B. A., and Engelman, D. M. (1983) *J. Mol. Biol. 166*, 211−217.
32. De Planque, M. R. R., Kruijtzer, J. A., Liskamp, R. M. J., Marsh, D., Greathouse, D. V., Koeppe, R. E., II, de Kruijff, B., and Killian, J. A. (1999) *J. Biol. Chem. 274*, 20839−20846.
33. Rinia, H. A., Demel, R. A., van der Eerden, J. P. J. M., and de Kruijff, B. (1999) *Biophys. J. 77*, 1683−1693.
34. Bloom, M, and Smith, I. C. P. (1985) in *Progress in Protein−Lipid Interactions*, Eds. (Watts, A., and De Pont, J. J. H. H. M., Eds.) pp 61−88, (Elsevier, Amsterdam.
35. Nielsen, C., Goulian, M., and Andersen, O. S. (1998) *Biophys. J. 74*, 1966−1983.
36. Dan, N., and Safran, S. A. (1998) *Biophys. J. 75*, 1410−1414.
37. Cahn, J. W. (1968) *Trans. Metall. Soc. AIME 242*, 166.
38. Seul, M., and Andelman, D. (1995) *Science 267*, 476−483.
39. Vlot, M. J., and van der Eerden, J. P. J. M. (1998) *J. Chem. Phys. 109*, 6043−6050.
40. Spisni, A., Pasquali-Ronchetti, I., Casali, E., Lindner, L., Cavatorta, P., Masotti, L., and Urry, D. W. (1983) *Biochim. Biophys. Acta 732*, 58−68.

BI000010C